Numerical and Analytical Modeling of Solid–Liquid Expression from Soft Plant Materials

Mykhaylo Petryk
Laboratoire de Modélisation du Transfert de Masse en Milieux Hétérogènes et Nanopores, Université Nationale Technique Ivan PULU'Y de Ternopil, 56, rue Ruska, 46001, Ternopil, Ukraine

Eugene Vorobiev
Laboratoire de Génie des Procédés Industriels, Centre de Recherches de Royallieu, Université de Technologie de Compiègne, BP 20.529 - 60205, Compiègne cedex, France

DOI 10.1002/aic.14213
Published online September 17, 2013 in Wiley Online Library (wileyonlinelibrary.com)

A physical model of solid–liquid expression from liquid containing plant materials is presented in one-dimensional (1-D) formulation. The layer of sliced cellular material is conceptualized as a double porosity system with extraparticle and intraparticle networks for liquid flow. Filtration-consolidation equations with corresponding initial and boundary conditions were formulated for both extraparticle and intraparticle networks. It was supposed for the sliced plant material that the extraparticle network forms the first porosity with low-storage capacity, while the intraparticle network forms a second porosity with high storage capacity. Computational modeling of pressure profiles in macro- and micropores versus time for different layer sections was done for real plant material (sugar beet tissue) with two different compressibility-permeability characteristics corresponding to different degrees of tissue disruption. Results demonstrate the delayed pressure drop in the intraparticle network and retardation of consolidation kinetics for the less destroyed plant tissue. © 2013 American Institute of Chemical Engineers *AIChE J*, 59: 4762–4771, 2013
Keywords: food processing, separations, solid–liquid expression, porous media, consolidation, mathematical modeling

Intoduction

Solid–liquid expression of biological materials is an important unit operation in the food and related industries, which is used for the extraction of fruit juices, vegetable oils, dehydration of fibrous materials, dewatering of wastewater sludge and so forth.[1]

During expression, the porous layer (press-cake) formed by a whole fruit (grape, berry) or fragmented material (e.g., sugar beet slices, apple mash, or ground oilseed) is subjected to unidirectional or complex compression in industrial presses (hydraulic, screw, belt-presses, etc). Such compression can be carried out under constant or variable parameters (pressure, deformation rate). Raw biological materials contain liquid filled cells, hydrated cell walls, microchannels between cells (plasmodesmata) and intercellular spaces containing air, i.e., are a porous media with different types of pores and channels.[1,2] Raw materials can be pretreated mechanically (slicing, grinding), thermally (heating, freezing-thawing) or by other methods (chemically, enzymes, pulsed electric field) to disrupt (denaturate) the cellular tissue and facilitate the further liquid expression.[1,3–6]

Evidently, the mechanisms of solid–liquid expression from a fresh raw material with initially intact cells and expression from the same material with initially disrupted cells are different. Cell breaking phenomena in a fresh tissue depend not only on the applied mechanical pressure and the rate of deformation, but also on the structural tissue characteristics (cell size and shape, thickness of the cell wall and the middle lamella, osmotic pressure inside a cell, etc.).[2] Intact cells can be broken individually or by groups (weakest cells first and then strongest ones) in the course of expression. Accordingly, liquid release from the fresh tissue depends on kinetics of cells destruction and can be slow. Intact cells remain impermeable and decrease the whole tissue permeability. In a fragmentized fresh tissue, just cell layers situated on the surface of particles are destroyed before expression. The portion of disrupted cells is lower in coarse particles (slices) and higher in finely fragmented material (mash). Therefore, expression kinetics depends significantly on the particle size.[1,7–9]

If the cell tissue is effectively pretreated and majority of cell membranes are destroyed before expression starts, then the whole tissue is permeable for the liquid flow. However, tissue structure can be affected differently by different pretreatments.

Apart from tissue permeability, the permeability of extraparticle pathways (channels) substantially affects the solid–liquid expression behavior. These interparticle channels are very compressible and can be completely or partly closed during expression, especially in the case of plate-like or very fine particles.

Air enclosed inside the tissue structure (mainly in the intercellular spaces) and outside the fragmentized particles

Correspondence concerning this article should be addressed to M. Petryk at Mykhaylo_Petryk@tu.edu.te.ua.

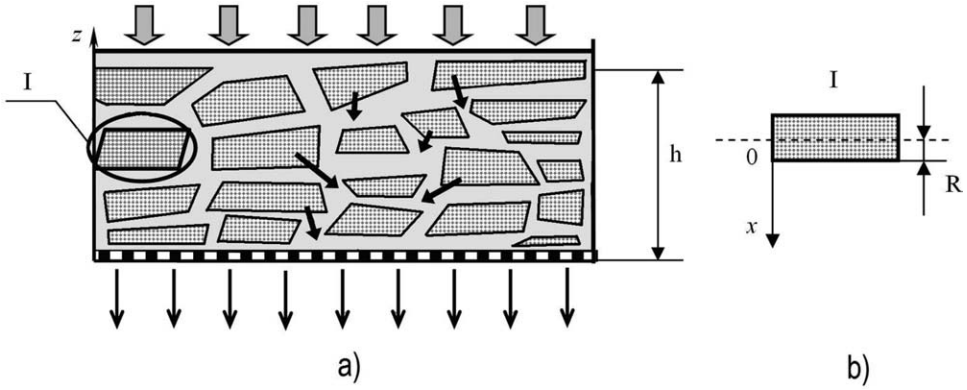

Figure 1. Scheme of mass transfer in double porosity system (a) layer, and (b) particle.

increases the compressibility of press-cake and also influences the *expression kinetics*.

Therefore, the mechanism of solid–liquid expression from biological materials is very complex. It is not completely understood yet. Currently, most of articles on simulation of the mechanical expression of cellular materials, adopt the filtration/consolidation theory developed for soils[10,11] and mineral filter cakes.[12–14] This theory gives a comprehensive approach for description of liquid flow inside compressible porous materials based on the analogy with Fick's diffusion theory. The consolidation coefficient b (m^2/s), which characterizes the pressure conductivity of a porous medium, bears analogy to diffusivity and thermal diffusivity coefficients. This analogy was the source for many studies on simulation of solid–liquid expression from biological materials.[1,15–18]

However, when mechanical pressure is applied to sliced or ground material, both soft tissue particles and the spaces between particles compact. It remains unclear what is the contribution of each layer component (soft particles and extraparticle channels) to the total layer compressibility-permeability. Compression behavior becomes more complicated and the complex mathematical models were proposed to estimate the consolidation and creep characteristics of layer components.[15,18] Consolidation coefficients for certain kinds of individual particles have recently been provided,[9,19] and in particular the values of consolidation coefficient b were determined experimentally for the individual tissue particles. Consequently, more realistic modeling of the solid–liquid expression from biporous layer (porous particles and extraparticle channels) can be realized considering particles and total layer deformation.[20]

In this article, analytical and numerical modeling of solid–liquid expression from biporous biological materials is presented and retardation phenomena are demonstrated for pressure distribution inside the porous particles.

Mathematical Formulation of the Problem

We consider sliced cellular particles containing liquid as a porous layer subjected to unidimensional pressing (Figure 1). Liquid flows inside the particles (intraparticle space), outside the particles (extraparticle space) and between these two spaces. The sliced particles are rectangular parallelepipeds separated by the porous network. The layer of sliced particles is considered as a double-porosity medium. The extraparticles network forms the first porosity with low-storage capacity and high-hydraulic permeability. The sliced liquid containing particles form a second porosity with high-storage capacity and low-hydraulic permeability. Flow occurs separately through the two porosities and between them. Figure 1 illustrates two scales of a representative elementary volume (a) layer scale 1 shows the extraparticles network, and (b) the particle scale 2 shows the porous medium of sliced particles. Discrete and continuum conceptualisations of a double-porosity medium are well described in the rock mechanics applied to the network of fissures in naturally fractured reservoirs.[21–23]

Main assumptions

The problem is stated based on the continuity equations and Darcy filtration law for both extraparticle and intraparticle spaces. Consolidation equations are formulated considering initial and boundary equations for the double porosity system. The assumptions are:

a. Consolidation behavior is studied after the initial compaction stage of expression when both intraparticle and extraparticle spaces are filled with liquid and compressed under a constant external pressure P_E.[15]

b. Continuity equations for the liquid phase in the extraparticle and intraparticle spaces are, respectively

$$\frac{\partial \varepsilon_1}{\partial t} + \frac{\partial \bar{\varepsilon}_2}{\partial t} + \frac{\partial q_1}{\partial z} = 0 \tag{1}$$

$$\frac{\partial (1-\varepsilon_1)}{\partial t} + \frac{\partial (1-\bar{\varepsilon}_2)}{\partial t} + \frac{\partial v_1}{\partial z} = 0 \tag{2}$$

c. Continuity equations for the liquid and solid phase in the intraparticle space are, respectively

$$\frac{\partial \varepsilon_2}{\partial t} + \frac{\partial q_2}{\partial x} = 0 \tag{3}$$

$$\frac{\partial (1-\varepsilon_2)}{\partial t} + \frac{\partial v_2}{\partial x} = 0 \tag{4}$$

where ε_1, ε_2 are, respectively the extraparticle and intraparticle porosities, and $\bar{\varepsilon}_2$ is the average intraparticle porosity $\bar{\varepsilon}_2 = \frac{1}{R}\int_0^R \varepsilon_2(t,x,z)dx$, q_1 and q_2 are, respectively, the local liquid velocities in the extraparticle and intraparticle spaces, v_1 and v_2 are respectively the local solid velocities in the extraparticle and intraparticle spaces.

d. Relatives liquid to solid flow velocities in the extraparticle (u_1) and intraparticle (u_2) spaces obey the Darcy filtration law

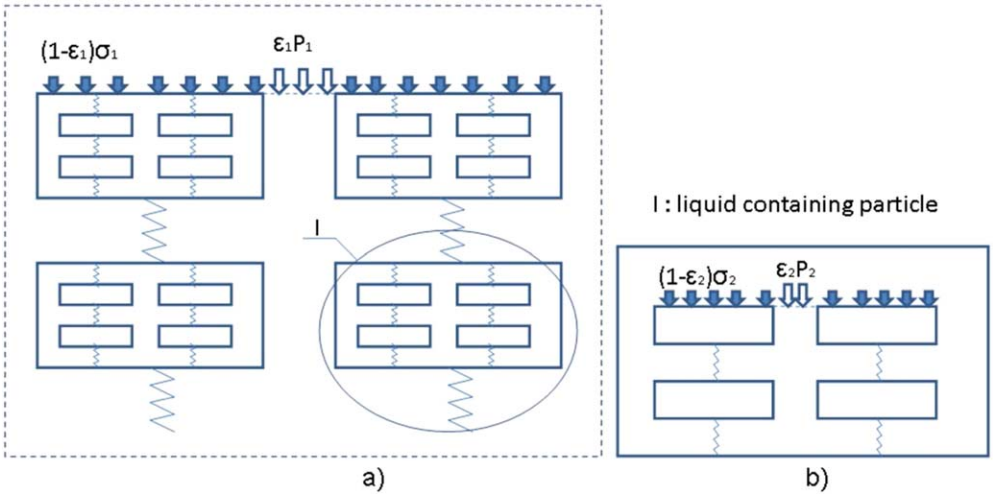

Figure 2. Total external stress (a) in extra particle network, and (b) in intraparticle network.

[Color figure can be viewed in the online issue, which is available at wileyonlinelibrary.com.]

$$u_1 = q_1 - \frac{\varepsilon_1}{1-\varepsilon_1} v_1 = -\frac{k_1}{\mu}\frac{\partial P_1}{\partial z} \tag{5}$$

$$u_2 = q_2 - \frac{\varepsilon_2}{1-\varepsilon_2} v_2 = -\frac{k_2}{\mu}\frac{\partial P_2}{\partial x} \tag{6}$$

where P_1 and P_2 are, respectively the liquid pressures in the extraparticle and intraparticle spaces, k_1 and k_2 are respectively the permeabilities of the extraparticle and intraparticle spaces, and μ is the liquid viscosity.

The contacts between liquid containing cellular particles are supposed to be elastic (springs). The compressibility of each particle is also supposed to be elastic (Figure 2a,b). Total external stress (σ) in the extraparticle network (Figure 2a)

$$\sigma = (1-\varepsilon_1)\sigma_1 + \varepsilon_1 P_1 \tag{7}$$

where σ_1 is the stress on the liquid containing cellular (soft) particles. The fictitious (effective or drag) pressure on the particles is defined as a difference between the total stress σ and the liquid pressure in pores.[15,21] In the case of biporous system the effective pressure on the liquid containing particles is

$$P_{s1} = \sigma - P_1 = (1-\varepsilon_1)(\sigma_1 - P_1) \tag{8}$$

Total external stress in the intraparticle network (Figure 2b)

$$\sigma_1 = (1-\varepsilon_2)\sigma_2 + \varepsilon_2 P_2 \tag{9}$$

where σ_2 is the stress on the solid matrix of liquid containing particles. The fictitious (effective) pressure on the solid matrix of liquid containing particles is defined as

$$P_{s2} = \sigma_1 - P_2 = (1-\varepsilon_2)(\sigma_2 - P_2) = P_1 + \frac{\sigma - P_1}{1-\varepsilon_1} - P_2 \approx \sigma - P_2 \tag{10}$$

The approximation in the right side of Eq. 10 is valid for the extraparticle space with a low-storage capacity $\varepsilon_1 \ll 1$.[23] The total stress σ is induced by the external pressure P_E, so $\sigma = P_E$. Then $P_{s1} = P_E - P_1$ and $P_{s2} = P_E - P_2$.

f. Replacing porosities ε_1 and ε_2 on the volume ratios $e_1 = \frac{\varepsilon_1}{1-\varepsilon_1}, e_2 = \frac{\varepsilon_2}{1-\varepsilon_2}, \bar{e}_2 = \frac{\bar{\varepsilon}_2}{1-\bar{\varepsilon}_2}$, and using the coordinates based on the volume of liquid containing particles (LCP) $dz_m = \frac{dz}{1+e_1}$, and insoluble solids (IS) $dx_m = \frac{dx}{1+e_2}$, one can modify the continuity Eqs. 1–4 considering Eqs. 5 and 6

$$\frac{\partial e_1}{\partial t} + \frac{1}{(1+\bar{e}_2)^2}\frac{\partial \bar{e}_2}{\partial t} + \frac{\partial u_1}{\partial z_m} = 0 \tag{11}$$

$$\frac{\partial e_2}{\partial t} + \frac{\partial u_2}{\partial x_m} = 0 \tag{12}$$

g. Additionally, we suppose that the average intraparticle porosity is a function of the average effective pressure $\bar{P}_{s2} = P_E - \bar{P}_2$, where $\bar{P}_2$ is the average liquid pressure inside the cellular particles $\bar{P}_2 = \frac{1}{R}\int_0^R P_2(t,x,z)dx$. Then

$$\frac{\partial e_1}{\partial t} = \frac{\partial e_1}{\partial P_{s1}}\frac{\partial P_{s1}}{\partial t} = \frac{1}{G_1}\frac{\partial P_1}{\partial t} \tag{13}$$

$$\frac{\partial e_2}{\partial t} = \frac{\partial e_2}{\partial P_{s2}}\frac{\partial P_{s2}}{\partial t} = \frac{1}{G_2}\frac{\partial P_2}{\partial t} \tag{14}$$

$$\frac{\partial \bar{e}_2}{\partial t} = \frac{\partial \bar{e}_2}{\partial \bar{P}_{s2}}\frac{\partial \bar{P}_{s2}}{\partial t} = \frac{1}{\bar{G}_2}\frac{\partial \bar{P}_2}{\partial t}, \tag{15}$$

where $G_1 = -\frac{\partial P_{s1}}{\partial e_1}$, $G_2 = -\frac{\partial P_{s2}}{\partial e_2}$, $\bar{G}_2 = -\frac{\partial \bar{P}_{s2}}{\partial \bar{e}_2}$ are the compressibility modulus.

Substituting Eqs. 5, 13 and 15 into Eq. 11, and using the coordinates based on the volume of liquid containing particles (LCP), we obtain a consolidation equation for the extraparticle space (problem A). Substituting Eqs. 6 and 14 into Eq. 12, and using the coordinates based on the volume of insoluble solids (IS), we obtain a consolidation equation for the intraparticle space (problem B).

Problem A: For the domain D_1, one should find the solution of the following equation of consolidation for extraparticles space

$$\frac{\partial P_1}{\partial t} = b_1 \frac{\partial^2 P_1}{\partial z_m^2} - \beta \frac{\partial \bar{P}_2}{\partial t} \tag{16}$$

Domain $D_1 = \{(t, z_m) : t > 0, 0 < z_m < h_m\}$

The initial condition is

$$P_1(t, z_m)|_{t=0} = P_E \tag{17}$$

The boundary conditions are

$$P_1(t, z_m)|_{z_m=0} = 0, \tag{18}$$

$$\frac{\partial P_1}{\partial z_m}|_{z_m=h_m} = 0 \quad \text{(absence of flow)}; \tag{19}$$

***Problem B*:** For the domain D_2, one should find the solution of the following equation of consolidation in intraparticle space

$$\frac{\partial P_2}{\partial t} = b_2 \frac{\partial^2 P_2}{\partial x_m^2}, \tag{20}$$

Domain z_m $D_2 = \{(t, x_m, z_m) : t > 0, |x_m| < R_m, 0 < z_m < h_m\}$
The initial condition is

$$P_2(t, x_m, z_m)|_{t=0} = P_E. \tag{21}$$

The boundary conditions are

$$\left.\frac{\partial P_2}{\partial x}\right|_{x_m=0} = 0 \quad \text{(symmetrical condition)}, \tag{22}$$

$$P_2(t, x_m, z_m)|_{x=R_m} = P_1(t, z_m). \tag{23}$$

where $b_1 = \frac{G_1}{\mu\alpha_1}$ is the consolidation coefficient of the extraparticles space, $b_2 = \frac{G_2}{\mu\alpha_2}$ is the consolidation of cellular particles, $\alpha_1 = \frac{1+e_1}{k_1}$ is the specific resistance of the extraparticles space based on the volume of LCP, and $\alpha_2 = \frac{1+e_2}{k_2}$ is the specific resistance of the intraparticle space (cellular particles) based on the volume of IS $\beta = \frac{1}{(1+\bar{e}_2)^2}\frac{G_1}{G_2}$, is the elasticity factor of the material h_m, is the thickness of IS layer $h_m = \int_0^h \frac{dz}{1+e_1}$, R_m is the thickness of the half of particle containing IS $R_m = \int_0^R \frac{dx}{1+e_2}$.

In Eqs. 16 and 20 it is assumed that b_1, b_2, and β are the constants. Variables k_1, k_2 can markedly decrease during pressing and α_1, α_2 can markedly increase. However, if G_1 and G_2 also increase in similar fashion, b_1 and b_2 will remain constant.

Deformation of Press-Cake and Consolidation Ratio

Total height reduction of the press-cake representing the liquid removed or the cumulative filtrate per unit area is given by

$$S(t) = S_1(t) + S_2(t) \tag{24}$$

where $S_1(t)$ and $S_2(t)$ are, respectively the height reductions of the extraparticle and intraparticle spaces

$$S_1(t) = \frac{1}{G_1}\int_0^{h_m} P_{s1}\, dz_m = \frac{1}{G_1}\int_0^{h_m} (P_E - P_1(t, z_m))\, dz_m \tag{25}$$

$$S_2(t) = \frac{1}{\bar{G}_2}\int_0^{h_m} \bar{P}_{s2}\, dz_m = \frac{1}{\bar{G}_2}\int_0^{h_m} (P_E - \bar{P}_2(t, z_m))\, dz_m. \tag{26}$$

In Eqs. 25 and 26 it is assumed that G_1 and $\bar{G}_2$ are the constants.

The consolidation ratio is defined as[11,12,15]

$$U = \frac{S(t)}{S_\infty} \tag{27}$$

where S_∞ is the final height reduction of press-cake at infinitively long time ($t = \infty$). In a fresh raw material, the liquid is mainly situated inside of cellular particles, and the total deformation of a liquid saturated layer can be mainly attributed to the deformation of soft particles. To calculate the consolidation ratio U we suppose additionally $1 + e_1 \cong 1 + \bar{e}_1$. Then

$$U(t) = \frac{S_2(t)}{S_\infty} \approx \frac{\int_0^{h_m} (P_E - \bar{P}_2(t, z_m))\, dz_m}{\int_0^{h_m} (P_E - \bar{P}_2(\infty, z_m))\, dz_m} \tag{28}$$

Analysis of Computational Modeling Results

Algorithm of the solution

An implicit finite difference method is used for the solution of a formulated mathematical model. A detailed description of the solution method is presented in Appendix .

Analysis of the solution

Using obtained numerical solutions; one can calculate the liquid pressure distributions inside of porous particles and in the extraparticle space. The next values of solid–liquid expression parameters were used for the calculation procedure: $h = 0.01$ m, $R = 0.004$ m, $b_1 = 1.8 \cdot 10^{-7}$ m^2/s, $b_2 = 10^{-7}$ m^2/s and 3.10^{-8} m^2/s, $\beta = 0.08$. The value of $b_2 = 10^{-7}$ m^2/s corresponds to the better disrupted tissue, while the value of $b_2 = 3.10^{-8}$ m^2/s corresponds to the less disrupted tissue. The values of b_2 can be determined using the procedure[9] for the individual tissue particles by the method of Sivaram and Swam[24] modified by Shirato.[25] The value of b_1 was chosen arbitrarily to show the possible deviation of the results estimated for the double-porosity system in compare to the single-porosity system. For all graphs we use the normalized values of liquid pressure $P_1^* = \frac{P_1}{P_E}$, $P_2^* = \frac{P_2}{P_E}$. The pressure distribution curves are presented in function of time and dimensionless geometrical coordinates $X = x_m/R_m$ and $Z = z_m/h_m$

Figure 3 is a set of plots of $P_2^*(t, X, Z)$, the dimensionless liquid pressure inside particles, vs. time t [s] for $b_2 = 10^{-7}$ m^2/s. Figure 3a shows $P_2^*(X)$ at Z = 0, the bottom of the layer (i.e., surface of the filter media); 3b $P_2^*(X)$ at Z = 0.05; 3c $P_2^*(X)$ at Z = 0.5; and 3d $P_2^*(X)$ at Z = 1 (the top of the layer). Figure 4a–d are a similar set of plots for $b_2 = 3.10^{-8}$ m^2/s. Curves 1–6 in each figure of these sets depict P_2^* vs. t at X = 1.0, 0.8, 0.6, 0.4, 0.05 and 0, respectively. In both Figures 3 and 4, P_2^* decreases more rapidly near the surface of the particles, X = 1, than at their center X = 0. The rate of decrease at X = 0 is slower at the top of the layer Z = 1, than near its bottom Z = 0, and is markedly slower for $b_2 = 3.10^{-8}$ m^2/s than for $b_2 = 10^{-7}$ m^2/s. For example, at Z = 0.5, the center of the layer P_2^* at X = 0 decreases from 1.0 to 0.2 in 420 s for $b_2 = 10^{-7}$ m^2/s, whereas for $b_2 = 3.10^{-8}$ m^2/s, P_2^* at X = 0 and Z = 0.5 decreases only to 0.45 when $t = 420$ s.

Therefore, the degree of disruption of cellular tissue can influence importantly on the pressure profiles and retardation of pressure drops inside the porous particles.

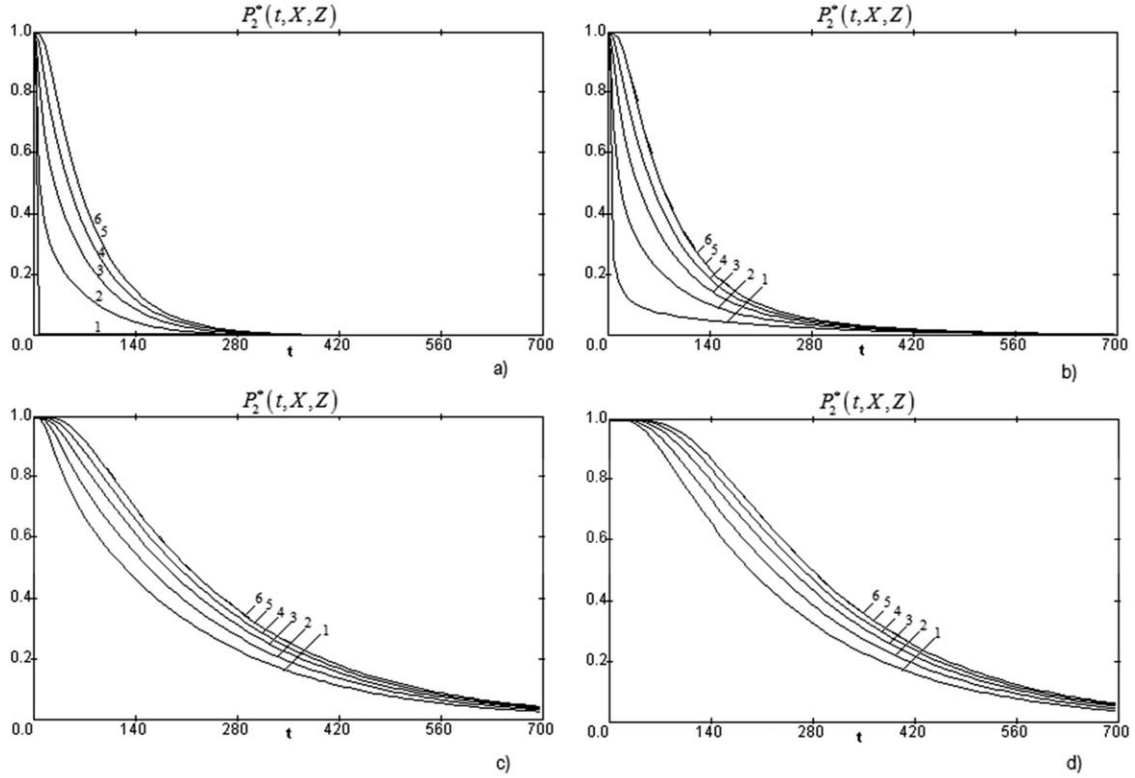

Figure 3. Temporal profiles of dimensionless pressure in the intraparticles space $P_2^*(t,X,Z)$ vs. time t, [s] for value $b_2 = 10^{-7}$ m^2/s, and different sections of layer (a) Z = 0.0, (b) Z = 0.05, (c) Z = 0.5, (d) Z = 1.

1 - X = 1.0 2 - X = 0.8; 3 - X = 0.6; 4 - X = 0.4; 5 – X = 0.05, 6 - X = 0.0.

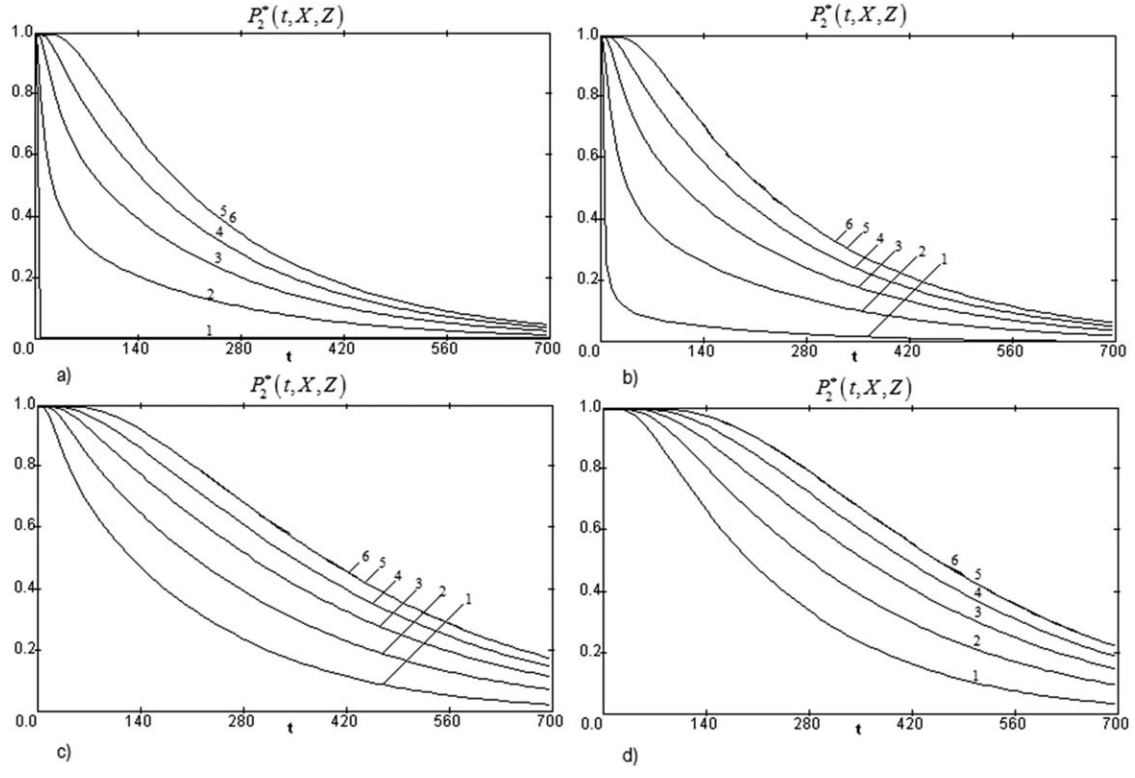

Figure 4. Temporal profiles of dimensionless pressure in the intraparticles space vs. time t, [s] for value $b_2 = 3.10^{-8}$ m^2/s different sections of layer (a) Z = 0.0, (b) Z = 0.05, (c) Z = 0.5, and (d) Z = 1.

1 - X = 1.0 2 - X = 0.8; 3 - X = 0.6; 4 - X = 0.4; 5 - X = 0.05, 6 - X = 0.0.

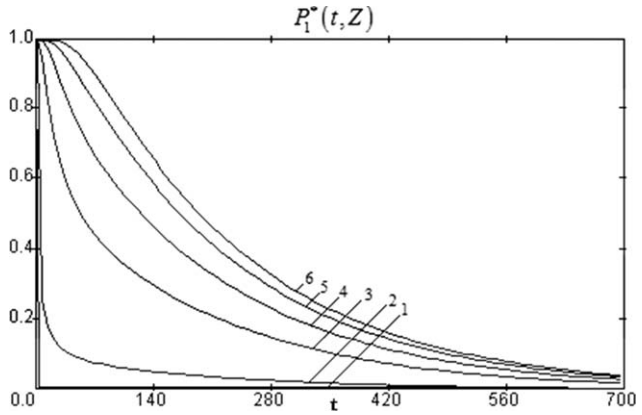

Figure 5. Model profiles of dimensionless pressures in extraparticle space vs. time *t*,[s] for value $b_2 = 10^{-7}$ m^2/s and different values of dimensionless layer thickness Z.

1 - Z = 0.0, 2 - Z = 0.05, 3 - Z = 0.3, 4 - Z = 0.5, 5 - Z = 0.7; 6 - Z = 1.0.

Figure 5 presents the temporal profiles of dimensionless pressure in macropores (extraparticles space) $P_1^*(t,Z)$ vs. time t[s] for the value of $b_2 = 10^{-7}$ m^2/s. Liquid pressure drops more rapidly near the surface of a filter medium, and there is some retardation with a pressure fall on the top of particles layer (Z = 1). When X tends to 1, the pressure in micropores tends to the pressure in macropores $P_1^*(t,Z)$. For instance, curve 1 for $P_2{}^*$ at X = 1, Z = 0 (Figure 3a) corresponds to curve 1 for $P_1{}^*$ at Z = 0 (Figure 5); curve 1 for $P_2{}^*$ at X = 1, Z = 0.5 (Figure 3c) corresponds to curve 4 for $P_1{}^*$ at Z = 0.5 (Figure 5); curve 1 for $P_2{}^*$ at X = 1, Z = 1 (Figure 3d) corresponds to curve 6 for $P_1{}^*$ at Z = 0.5 (Figure 5).

Figure 6 presents the temporal profiles of dimensionless pressure in macropores (extraparticles space) $P_1^*(t,Z)$ vs. time t[s] for the value of $b_2 = 3.10^{-8}$ m^2/s. It is possible to see that curve 1 for $P_2{}^*$ at X = 1, Z = 0 (Figure 4a) corresponds to curve 1 for $P_1{}^*$ at Z = 0 (Figure 6); curve 1 for $P_2{}^*$ at X = 1, Z = 0.5 (Figure 4c) corresponds to curve 4 for $P_1{}^*$ at Z = 0.5 (Figure 6); curve 1 for $P_2{}^*$ at X = 1, Z = 1 (Figure 4d) corresponds to curve 6 for $P_1{}^*$ at Z = 0.5 (Figure 6).

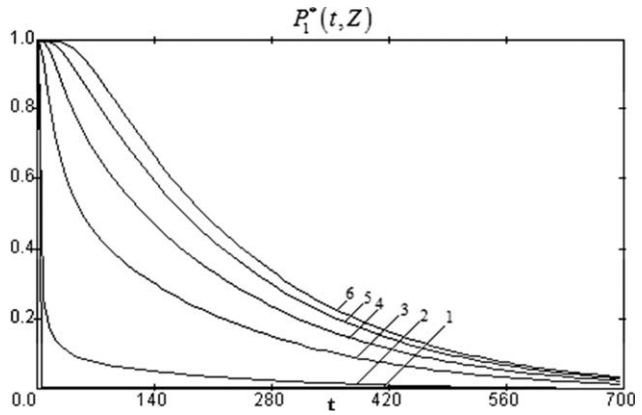

Figure 6. Model profiles of dimensionless pressures in extraparticle space $P_1^*(t,Z)$ vs. time *t*,[s] for the value of $b_2 = 3.10^{-8}$ m^2/s and different values of dimensionless layer thickness Z.

1 - Z = 0.0, 2 - Z = 0.05, 3 - Z = 0.3, 4 - Z = 0.5, 5 - Z = 0.7; 6 - Z = 1.0.

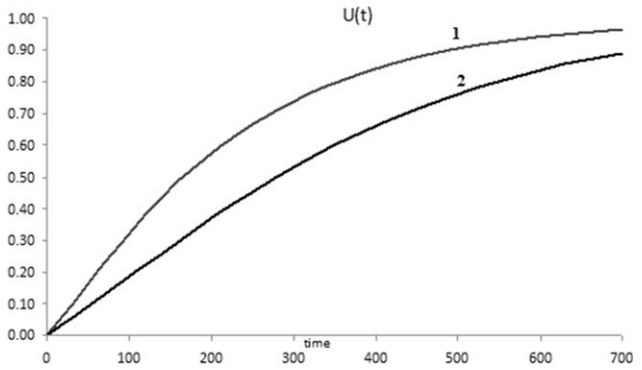

Figure 7. Consolidation ratio *U*(*t*) simulated using two different values of b_2.

(1) $b_2 = 10^{-7}$ m^2/s, and (2) $b_2 = 3.10^{-8}$ m^2/s.

Pressure profiles in the extraparticle space $P_1{}^*$ have a similar behavior for both layers formed by less and better disrupted particles (Figures 5 and 6). This is despite difference in pressure profiles $P_2{}^*$ inside of less and better destroyed particles (Figures 3 and 4). It means that the permeability of the extraparticle space remains sufficient to evacuate similarly the liquid from better and less disrupted particles. For particles and extraparticle space with other permeability-compressibility characteristics, the pressure profiles $P_1^*(t,Z)$ can differ. Simulation shows that the dependence of profiles $P_1^*(t,Z)$ on the values of b_2 is more important for the higher values of elasticity factor ($\beta > 0.08$).

Figure 7 presents the curves of the consolidation ratio $U(t)$ simulated using Eq. 24 for the values of $b_2 = 10^{-7}$ m^2/s (curve 1) and $b_2 = 3.10^{-8}$ m^2/s (curve 2). As can be seen from Figure 7, the consolidation kinetics is more rapid for the better destroyed plant tissue ($b_2 = 10^{-7}$ m^2/s).

In the article,[10] it was indicated that both filtration/consolidation and creep effects influence on the expression behavior of sugar beets. However, Eq. 20 of this work describes just the filtration/consolidation behavior of this material. It can be the source of some deviation between experimental and calculated results.

Comparison of numerical and analytical solutions

Figure 8 presents the temporal profiles of dimensionless pressure in macropores simulated by numerical and analytical methods for the value of $b_2 = 10^{-7}$ m^2/s. As can be seen, the pressure profiles computed by analytical method (formula B.1, curve 1) correspond well with the numerical solution (curve 2) for different layer sections (Z = 0.2, Z = 0.5, and Z = 0.8). The lack of convergence between the analytical and the numerical solutions is between 1.5 and 2% for all three sections of layer.

Figure 9 presents the temporal profiles of dimensionless pressure in micropores of particles simulated by numerical and analytical methods for the value of $b_2 = 10^{-7}$ m^2/s. As can be seen, the pressure profiles computed by analytical method (formula B.2, curve 1) correspond well with the numerical solution (curve 2) for two different sections of particle (X = 0.5 and X = 0.7) taken for two positions in layer: Z = 0.2 (Figure 9a) and Z = 0.8 (Figure 9b). In both cases the lack of convergence between the analytical and numerical solutions does not exceed 2.0%.

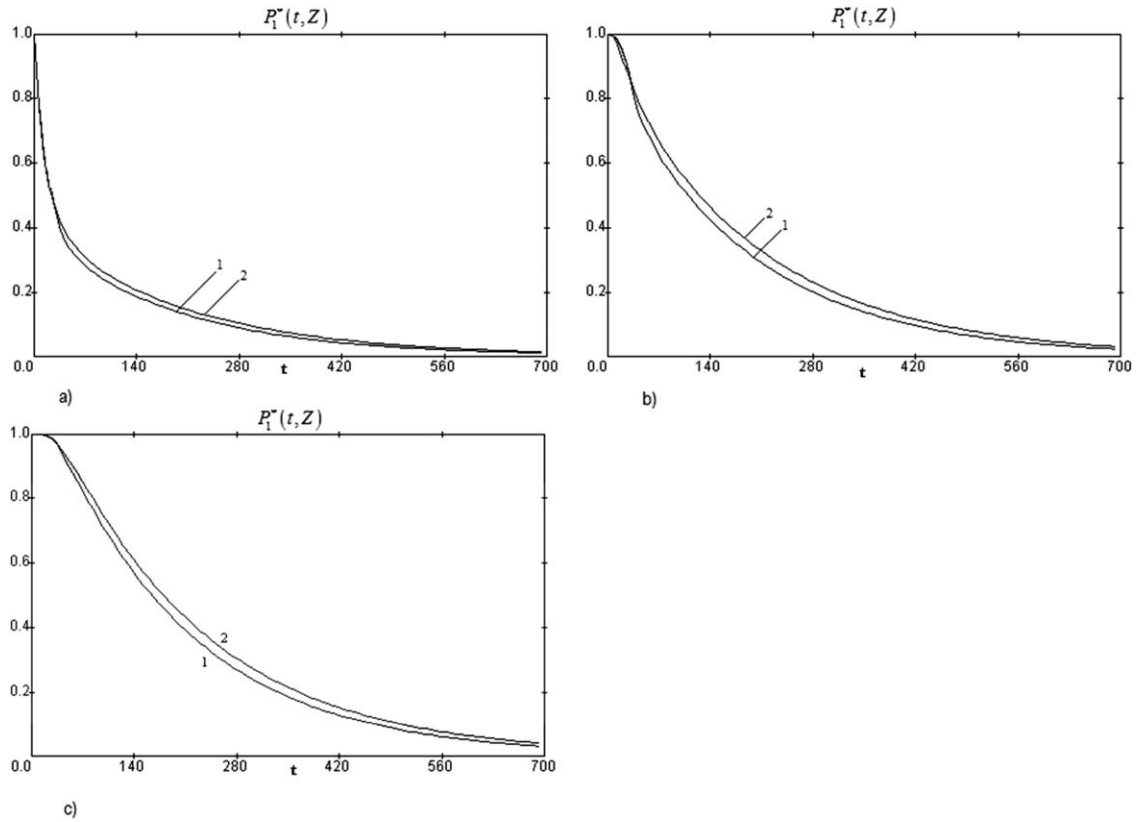

Figure 8. Comparison of pressure profiles for extraparticle space $P_1^*(t,Z)$ in time for analytical (1) and numerical (2) solutions of model.

(a) Z = 0.2, (b) Z = 0.5, and (c) Z = 0.8.

The analytical solution has advantages for the physical analysis of functional dependencies between the parameters of solid–liquid expression (b_1, b_2 and β), and obtained pressure profiles $P_2^*(t,X,Z)$, $P_1^*(t,Z)$ and consolidation ratio $U(t)$. The numerical method is computationally more expensive, but can facilitate future evaluation of alternative processing conditions (e.g., variable pressure) and pressing parameters.

Conclusions

Phenomenological model of solid–liquid expression from liquid containing plant materials is formulated representing the layer of sliced cellular particles as a biporous system with extraparticle and intraparticle networks for liquid flow. The filtration-consolidation equations were formulated for both extraparticle and intraparticle networks considering the pressure profiles. It was supposed for the sliced plant material that the extraparticles network forms the first porosity with low-storage capacity, while the intraparticle network form a second porosity with high-storage capacity. Numerical and analytical solutions for the temporal pressure profiles and for the consolidation ratio were obtained with two different compressibility-permeability characteristics corresponding to different degrees of tissue destroying.

The results show the delayed pressure drop in the intraparticle network and retardation of consolidation kinetics for the less destroyed plant tissue (due to the lower value of consolidation coefficient b_2). Experimental verification of obtained results for the plant tissue is still needed.

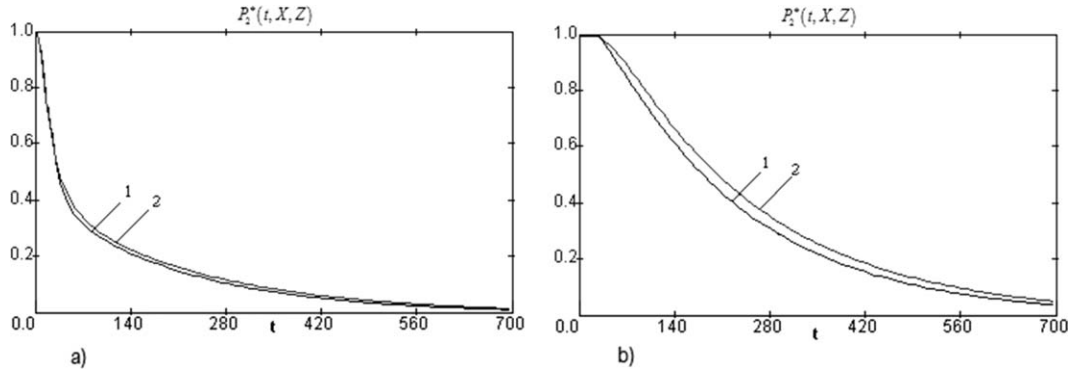

Figure 9. Comparison of pressure profiles for intraparticle space in time for analytical (1) and numerical (2) solutions of model.

(a) Z = 0.2, X = 0.5, and (b) Z = 0.8, X = 0.7.

Notation

b_1 = consolidation coefficient of the extraparticles space, m^2/s
b_2 = consolidation coefficient of the intraparticle space (cellular particles), m^2/s
e_1 = volume ratio of the extraparticle space
e_2 = volume ratio of the intraparticle space
$\bar{e}_2$ = average volume ratio of the intraparticle space
G_1 = compressibility modulus of the extraparticle space, Pa
G_2 = compressibility modulus of cellular particles, Pa
$\bar{G}_2$ = average compressibility modulus of cellular particles, Pa
h = layer thickness, m
k_1 = permeability of the extraparticle space,m^2
k_2 = permeability of the intraparticle space, m^2
P_1 = liquid pressure in the extraparticle space, Pa
P_2 = liquid pressure *i*-n the intraparticle space, Pa
P_E = external pressure, Pa
P_{s1} = effective pressure on the liquid containing particles, Pa
P_{s2} = effective pressure on the solid matrix of the liquid containing particles
$\bar{P}_2$ = average liquid pressure inside the cellular particles, Pa
$\bar{P}_{s2}$ = average efective pressure on the solid matrix of the liquid containing particles, Pa
P_1^* = normalized values of liquid pressure P_1
P_2^* = normalized values of liquid pressure P_2
q_1 = local liquid velocity in the extraparticle space, m/s
q_2 = local liquid velocity in the intraparticle space, m/s
R = particle half thickness, m
R_m = the thickness of the half of particle containing IS, m
S_1 = height reduction of the extraparticle space, m
S_2 = height reduction of the intraparticle space, m
S = total height reduction, m
S_∞ = final height reduction, m
t = time, s
Δt = the interval along the axe of time t
U = consolidation ratio
u_1 = local liquid to solid flow velocity in the extraparticle space, m/s
u_2 = local liquid to solid flow velocity in the intraparticle space,m/s
v_1 = local solid velocity in the extraparticle space,m/s
v_2 = local solid velocity in the intraparticle space,m/s
x = coordinate of the intraparticle space, m
x_m = coordinate of the intraparticle space based on the volume of IS per unit of area, m
X = dimensionless particle half thickness, $(X=x_m/R_m)$
z = coordinate of the extraparticle space, m
z_m = coordinate of the extraparticle space based on the volume of LCP per unit of area, m
Z = dimensionless layer thickness, $(Z=z_m/h_m)$
ΔX = the length of segments along the axe X
ΔZ = the length of segments along the axe Z
i, j, k, n = index
α_1 = specific resistance of the extraparticle spase, based on the volume of LCP, m^{-2}
α_2 = specific resistances of the intraparticle space m^{-2}, based on the volume of IS, m^{-2}
β = elasticity factor of the material
ε_1 = extraparticle porosity
ε_2 = intraparticle porosity
$\bar{\varepsilon}_2$ = average intraparticle porosity
μ = liquid viscosity, Pa.s;
σ_1 = total external stress in the intraparticle space, Pa
σ_2 = stress on solid matrix of liquid containing particles, Pa
σ = total external stress in the extraparticle space, Pa

Literature Cited

1. Schwartzberg HG. Expression of fluid from biological solids. *Sep Purif Methods*. 1997;26(1):1–213.
2. Zhuw HX, Melrosez JR. A mechanics model for the compression of plant and vegetative tissues. *J Theor Biol*. 2003;221:89–101.
3. Van Der Poel PW, Schiweck H, Schwartz T. Sugar Technology, Beet and Cane Sugar Manufacture. Berlin, Germany: Bartens; 1998.
4. Bliesener KM, Meihe D, Bucholoz K. Pressing of Cossettes after Alkaline Pre-Treatment. The XIX Assambly of the Commission Internationale Technique de Sucrerie. Cambridge, UK: CITS; 1991; 407–440.
5. Knorr D, Geulen M, Grahl T, Sitzmann W. Food application of high electric field pulses. *Trends Food Sci Technol*. 1994;5(3): 71–75.
6. Bouzrara H, Vorobiev E. Solid–liquid expression of cellular materials enhanced by pulsed electric field. *Chem Eng Proc*. 2003;42(4): 249–257.
7. Bazhal MI, Lebovka NI, Vorobiev E. Pulsed electric field treatment of apple tissue during compression for juice extraction. *J Food Eng*. 2001;50(3):129–139.
8. Vorobiev E, Lebovka N. Pulsed-electric-fields-Induced effects in plant tissues: fundamental aspects and perspectives of applications. In: Vorobiev E, Lebovka N, eds. Electrotechnologies for Extraction from Food Plants and Biomaterials. New York: Springer; 2008: 39–89.
9. Grimi N, Vorobiev E, Lebovka NI, Vaxelaire J. Solid–liquid expression from denaturated plant tissue: Filtration-consolidation behavior. *J Food Eng*. 2010;96(1):29–36.
10. Terzaghi K. Erdbaumechanik auf Bodenphysikalischer Grundlage. Wien, Germany: Deuticke; 1925.
11. Suclje L. Rheological Aspects of Soil Mechanics. New York: Wiley Interscience; 1970.
12. Shirato M, Murase T, Kato H, Fukaya S. Fundamental analysis for expression under constant pressure. *Filtr Sep*. 1970;7:277–282.
13. Shirato M, Murase T, Negawa M, Moridera H. Analysis of expression operations. *J Chem Eng Japn*. 1971;4:263–268.
14. Shirato M, Murase T, Iwata M, Nakatsuka S. The Terzaghi-Voigt combined model for constant pressure consolidation of filter cakes and homogeneous semi-solid materials. *Chem Eng Sci*. 1986;41: 3213–3218.
15. Lanoiselle JL, Vorobyov E, Bouvier JM, Piar G. Modelling of solid/liquid expression for cellular materials, *AIChE J*. 1996;42:N7:2057–2067.
16. Buttersack C. Two-zone model for solid–liquid separation by filtration and expression. *Chem Eng Sci*. 1994;49(8):1145–1160.
17. Rebouillat S, Campanella OH, Leclerc D. The expression under constant rate of strain and the subsequent relaxation. 7th World Filtration Congress. Budapest, Hungary; 1996;112–121.
18. Kamst GF, Bruinsma OSL, De Graauw J. Solid-phase creep during the expression of palm-oil filter cakes, *AIChE J*. 1997;43:665–672.
19. Grimi N, Lebovka N, Vorobiev E, Vaxelaire J. Compressing behaviour and texture evaluation for potatoes pretreated by pulsed electric field. *J Texture Studies*. 2009;40:208–224.
20. Petryk M, Vorobiev E. Liquid flowing from porous particles during the pressing of biological materials. *Comput Chem Eng*. 2007; 31(10):1336–1345.
21. Barenblatt GI. Entov VM. Ryzhik V. Theory of Fluid Flows through Natural Rocks. Dordrecht, Germany: Kluwer; 1990.
22. Dontsov KM, Boyarchuk VT. Effect of characteristics of fractured media on pressure buildup behavior. *Izv Vyssh Uchebn Zaved Neft i Gas*. 1971;1:42–46.
23. Buyevich YA, Nustrov VS. Nonliniar flow in fractured porous media. Transport in *Porous Media*. 1993;12:1–17.
24. Sivaram B, Swamee PK. A computational method for consolidation coefficient. *Japn Soc Soil Mech Found Eng*. 1977;17:48–52.
25. Shirato M, Murase T, Atsumi K. Simplified computational method for constant pressure expression of filter cakes. *J Chem Eng Japn*. 1980;13(5):397–401.
26. Bahvalov NS. Jytcov NP. Kobelkov GM. Numerical Methods. Moscow, Russia: Nauka; 1987.
27. Lenyuk M, Petryk M. The Methods of Integral Transformations of Fourier, Bessel with Spectral Parameter in Problems of Mathematical Modeling of the mass Exchange Process in no Regular Medias. Kyiv, Russia: Naukova Dumka; 2000.

Appendix A: Numerical Method

Implicit finite difference method[26] is used for the numerical solution. The scheme is presented in Figure A1. The IS layer thickness h_m is divided into N segments along the axe Z, the IS particle half-thickness R_m is divided into M segments along the axe X, and the time is divided into L intervals along the axe t.

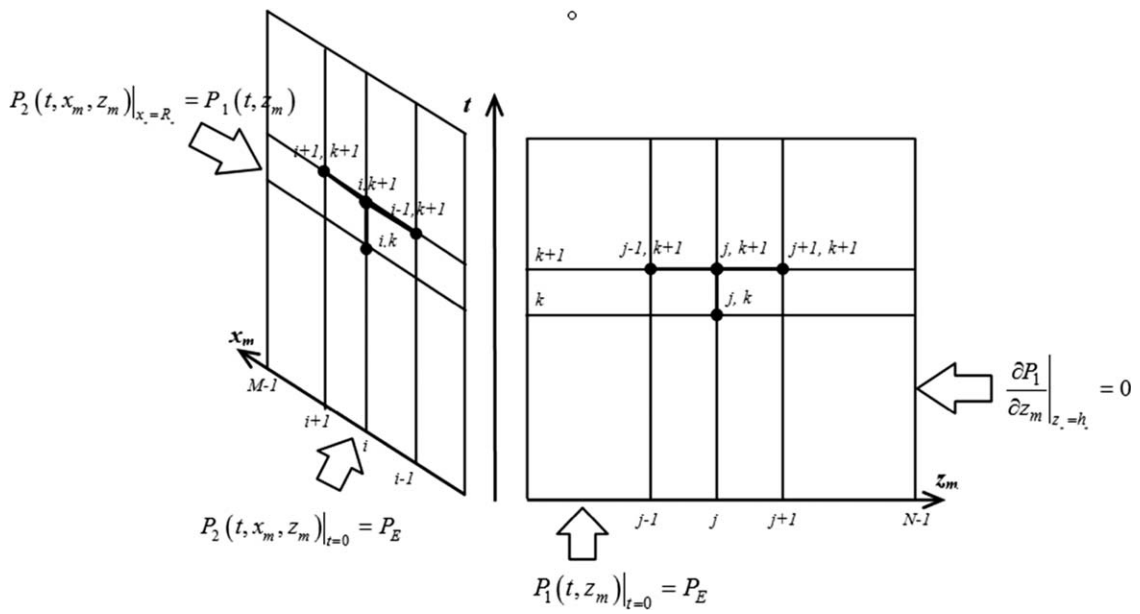

Figure A1. Grids area with finite difference template for model Eqs. 16–23.

As a result, the problem (16–23) is transformed to the next system of equations:

Problem A:

$$\frac{P_{1_j}^{k+1}-P_{1_j}^{k}}{\Delta t}=b_1\frac{h_m^2}{h^2}\cdot\frac{P_{1_{j-1}}^{k+1}-2P_{1_j}^{k+1}+P_{1_{j+1}}^{k+1}}{\Delta z_m^2}-\beta\frac{\bar{P}_{2_j}^{k+1}-\bar{P}_{2_j}^{k}}{\Delta t},\qquad k=1,\bar{L},\qquad j=1,\bar{N}-1 \tag{A.1}$$

Initial condition:

$$\left[P_{1_0}^{k}\right]_{k=1,\bar{L}}=P_E; \tag{A.2}$$

Boundary conditions:

$$\left[P_{1_0}^{k}\right]_{k=1,\bar{L}}=0;\qquad \frac{h_m}{h}\frac{1}{\Delta z_m}\left[P_{1_n}^{k}-P_{1_{n-1}}^{k}\right]_{k=1,\bar{L}}=0; \tag{A.3}$$

Problem B:

$$\frac{P_{2_{i,j}}^{k+1}-P_{2_{i,j}}^{k}}{\Delta t}=b_2\frac{R_m^2}{R^2}\cdot\frac{P_{2_{i-1,j}}^{k+1}-2P_{2_{i,j}}^{k+1}+P_{2_{i+1,j}}^{k+1}}{\Delta x_m^2}; \tag{A.4}$$

Initial condition:

$$\left[P_{2_{i,j}}^{0}\right]_{j=1,\bar{n}}=P_E; \tag{A.5}$$

Boundary conditions: $\frac{R_m}{R}\frac{1}{\Delta x_m}\left[P_{2_{1,j}}^{k}-P_{2_{0,j}}^{k}\right]_{j=0,\bar{N}\,k=1,\bar{L}}=0;$

$$\left[P_{2_{N,j}}^{k}\right]=\left[P_{1_j}^{k}\right]_{k=1,\bar{L}\,j=1,\bar{N}}; \tag{A.6}$$

Problem (A1–A6) can be presented as the next algebraic system

$$\delta_1 P_{1_{j-1}}^{k+1}-(1+2\delta_1)P_{1_j}^{k+1}+\delta_1 P_{1_{j+1}}^{k+1}=P_{1_j}^{k}-\beta\left(\bar{P}_{2_j}^{k+1}-\bar{P}_{2_j}^{k}\right); \tag{A.7}$$

$$\delta_2 P_{2_{i-1,j}}^{k+1}-(1+2\delta_2)P_{2_{i,j}}^{k+1}+\delta_2 P_{2_{i+1,j}}^{k+1}=P_{2_{i,j}}^{k};\ j=1,\bar{N}-1\ \ i=1,\bar{M}-1; \tag{A.8}$$

Matrices of the algebraic systems (A7–A8)

$$A_s=\begin{bmatrix}\delta_s & -(1+2\delta_s) & \delta_s & 0 & \dots & 0\\ 0 & \delta_s & -(1+2\delta_s) & \delta_s & \dots & \\ \dots & \dots & \dots & \dots & \dots & \dots\\ \dots & \dots & \dots & \dots & \dots & \dots\\ 0 & \dots & 0 & \delta_s & -1(1+2\delta_s) & \delta_s\end{bmatrix}_{s=1,\bar{2}}, \tag{A.9}$$

where $\delta_1=b_1\frac{h_m^2}{h^2}\frac{\Delta t}{\Delta z_m^2};\qquad \delta_2=b_2\frac{R_m^2}{R^2}\frac{\Delta t}{\Delta x_m^2}.$

The system (A9) was solved using tridiagonal matrix algorithm TDMA.[26] The value of average liquid pressure inside the cellular particles $\bar{P}_{2_j}^{k}(t,z_m)$ was determined by Simpson's method.[26]

Appendix B: Analytical Solution

Analytical solutions for the liquid pressure distribution inside of macropores (extraparticle space) $P_1(t,\ z_m)$, and micropores (intraparticle space) $P_2(t,\ x_m,z_m)$, were obtained by Petryk and Vorobiev[20] based on the methods developed by Lenyuk and Petryk.[27] These solutions have the next form

$$P_1(t,z_m)=P_E\sum_{n=0}^{\infty}\sum_{j=1}^{\infty}\phi_{jn}e^{-\frac{b_2}{R_m^2}Q_{jn}^2 t}\left[1-\beta\sum_{k=0}^{\infty}\frac{1-e^{-\frac{b_2}{R_m^2}N_k^2\left(1-\frac{Q_{jn}^2}{N_k^2}\right)t}}{1-\frac{Q_{jn}^2}{N_k^2}}\frac{2}{N_k^2}\right]\frac{\sin\left(L_n\frac{z_m}{h_m}\right)}{L_n}, \tag{B.1}$$

$$P_2(t,x_m,z_m)=P_1(t,z_m)+$$
$$+P_E\sum_{i=0}^{\infty}\left[\begin{array}{l} e^{-\frac{b_2}{R_m^2}N_i^2 t}+ \\ +\sum_{n=0}^{\infty}\sum_{j=1}^{\infty}\Phi_{jni}e^{-\frac{b_2}{R_m^2}Q_{jn}^2 t}\left[\begin{array}{l} 1-e^{-\frac{b_2}{R_m^2}N_i^2\left(1-\frac{Q_{jn}^2}{N_i^2}\right)t}- \\ -\beta\sum_{k=0}^{\infty}\frac{1-e^{-\frac{b_2}{R_m^2}N_i^2\left(1-\frac{Q_{jn}^2}{N_k^2}\right)t-\widehat{\omega}_{ikjn}}}{1-\frac{Q_{jn}^2}{N_k^2}}\frac{2}{N_k^2}\end{array}\right]\frac{\sin L_n\frac{z_m}{h_m}}{L_n}- \\ -P_1(t,z_m)/P_E\end{array}\right]\frac{2(-1)^i}{L_i}\cos N_i\frac{x_m}{R_m}. \quad \text{(B.2)}$$

Here

Q_{jn}, $n=1,\bar{\infty}$ are the roots of transcendental equation

$$Q^2-\frac{b_1}{b_2}\frac{R_m^2}{h_m^2}L_n^2+\beta Q\tan Q=0; \quad \text{(B.3)}$$

$$\phi_{jn}=\frac{2}{1+\frac{\beta}{2}\left(\frac{1}{Q_{jn}}\tan Q_{jn}+\frac{1}{\cos^2 Q_{jn}}\right)},\qquad \Phi_{jni}=\phi_{jn}/\left(1-\frac{Q_{jn}^2}{N_i^2}\right)$$

$$L_n=(2n+1)\frac{\pi}{2},\qquad N_i=(2i+1)\frac{\pi}{2},n,i=0,\bar{\infty};$$

$$\widehat{\omega}_{ikjn}=\left(1-\frac{Q_{jn}^2}{N_i^2}\right)\begin{cases}\dfrac{e^{-\frac{b_2}{R_m^2}N_i^2\left(1-\frac{Q_{jn}^2}{N_i^2}\right)t}-e^{-\frac{b_2}{R_m^2}N_k^2\left(1-\frac{Q_{jn}^2}{N_i^2}\right)t}}{1-\frac{N_k^2}{N_i^2}}, & i\neq k\\ \frac{b_2}{R_m^2}N_i^2 te^{-\frac{b_2}{R_m^2}N_i^2\left(1-\frac{Q_{jn}^2}{N_i^2}\right)t}, & i=k\end{cases}$$

To evaluate Eqs. B1 and B2, the values of Q_{jn} should be initially determined from the transcendental Eq. B3, where j is the index of internal summation, and n is the index of external summation. There is an infinite number of roots Q_j for each successive value of n. The nested series in (B1) and (B2) were evaluated by using the Qj for a given n to determine the ϕ_j, and other expressions (Φ_j, $\widehat{\omega}_j$) involving Qj for the j-based summation for that n (using only as many j as needed to cause the j-based summation to converge). Starting from $n=0$ and repeating this process for as many successive n as needed, the values of Q_{jn} are evaluated to cause the sum of the n, j-based summations to converge.

For good convergence of the series Eqs. B.1 and B.2, the number of j and n summations can be limited to 5–10. Authors used the first 20 members of the series in the numerical calculations.

The needed number of series terms to provide summation convergence is following: at t = 20s, $n=8-10$, $j=10-12$; at t = 50s, $n=6-8$, $j=8-10$; at t = 200s, $n=3-4$, $j=5-6$.

Manuscript received Aug. 31, 2012, and revision received July 16, 2013.